Preprints of the 21st IFAC World Congress (Virtual)
Berlin, Germany, July 12-17, 2020

Condition Monitoring for Single-Rotor Wind Turbine Load Sensors in the Full-Load Region

Thomas Thuesen Enevoldsen * **Roberto Galeazzi** *
Dimitrios Papageorgiou * **Christian Jeppesen** **

* *Department of Electrical Engineering, Technical University of Denmark, DK-2800 Kgs. Lyngby, Denmark, (e-mail: {tthen,rg,dimpa}@elektro.dtu.dk).*
** *Vestas Wind Systems Denmark (e-mail: chjpe@vestas.com)*

Abstract: Incipient faults on blade load sensors can impede the sound performance of a wind turbine, leading to increasing loads over time and severe blade degradation. As such, knowledge of the blade load sensors' health is essential for ensuring effective load reduction by means of individual pitch control. This paper presents a condition monitoring strategy for the blade load sensors based on estimation of the loads acting on the rotor blades in the full-load region. Fault detection is achieved via appropriate residual generators, the statistical properties of which are used to design change detectors robust against measurement noise and wind field stochasticity. Specifically, a Generalized Likelihood Ratio Test for the t-LocationScale distribution is developed for ensuring robust detection of sensor blade faults. The proposed method is evaluated in a high-fidelity simulator under non-uniform wind scenarios. The simulation results show that detection of multiplicative faults on the blade load sensors is achieved even in absence of knowledge of the local wind speed.

Keywords: Blade load sensor fault, Wind turbine, Condition monitoring, Filtering and change detection, Generalized likelihood ratio test, t-LocationScale distribution

1. INTRODUCTION

The increasing manufacturing cost of larger wind turbines that facilitate higher power production necessitates longer lifespan of the wind turbine structure. To this end, the use of Individual Pitch Control (IPC) has grown more popular since it ensures the same level of power production efficiency as well as it contributes to fatigue mitigation of the tower structure. However, corrupted blade load measurements hinder the effectiveness of the IPC loops and may lead to reduced power production, increased tower structure fatigue and, in extreme cases, significant damage of the blades. Therefore, detection and isolation of faults on the blade load sensors is fundamental for ensuring robust operation of the wind turbine and fatigue mitigation without compromising power production.

Wind turbine fault diagnosis has been widely investigated for years, where a well known benchmark challenge by Odgaard et al. [2009]; Odgaard et al. [2013] was used to specify common failure modes and remedial requirements for a general wind turbine. Efforts with emphasis on identifying and mitigating faults that occur within the blade load sensors are sparsely reported in the literature. Wei et al. [2008] modelled the wind turbine using a closed-loop system identification approach, such that the wind dynamics were included into the model. Both additive and multiplicative faults were investigated using mean and variance change detectors, respectively. However, the considered multiplicative faults were large in magnitude and redundancy of blade sensors was assumed to aid isolation. In Wei and Verhaegen [2011] the problem was addressed by designing a robust observer towards the wind disturbance. Sanchez et al. [2015] identified a polynomial relationship between the pitch angles and blade load sensors, where both the polynomial descriptions and the implemented fault detection scheme were validated using Fatigue, Aerodynamics, Structures, and Turbulence (FAST) software assuming uniform wind conditions. Niemann et al. [2018] exploited the Multiblade coordinate (MBC) transformation to detect and isolate faults occurring in the rotor subsystem using a model-free approach.

Common assumptions often adopted by previous works relate to the availability of accurate measurements of the local wind speed or validation during simple uniform wind scenarios. These hypotheses can be very conservative, since the availability of such information is typically limited, and assumptions of uniform wind falls short due to the highly stochastic profile of the local wind speed. It is often the case that the available wind measurements are considered unreliable, due to being obtained from an anemometer and representing only a single point of wind within the area covered by the rotor, whilst being heavily influenced by blade shadow. This paper proposes a method for detection of incipient faults in the blade load sensors of single-rotor wind turbines (SRT) in the full load region without assuming knowledge of the local wind speed. The blade loads are estimated using the tip-speed ratio and the individual pitch angles, and are subsequently used as inputs to residual generators for fault detection. Statistical change detection techniques have been proven to be a powerful tool for robustifying fault detection schemes against measurement noise and process stochastic uncertainty in industrial applications. A few characteristic examples can be found in Galeazzi et al. [2012, 2015]; Hansen and Blanke [2014]; Willersrud et al. [2015] and Ghane et al. [2018]. To account for the stochasticity of the wind field in the detection of the blade sensors faults, statistical analysis is carried out on the outputs of the designed residual generators and a detector based on the Generalized Likelihood Ratio Test (GLRT) for the t-LocationScale distribution is derived for monitoring changes in the residuals. High-fidelity simulations using

FAST, driven by non-uniform stochastic wind fields, demonstrate the efficacy of the proposed diagnostic scheme.

The rest of the paper is organized as follows: Section 2 describes the SRT system and formulates the problem at hand. Section 3 illustrates the proposed condition monitoring strategy for the blade load sensors. Section 4 presents the results obtained from simulations and evaluates the performance of the fault diagnosis algorithm. Finally, Section 5 draws some conclusions and points towards future research directions.

2. SYSTEM DESCRIPTION AND PROBLEM FORMULATION

2.1 Single-rotor wind turbine system

Consider a single-rotor, horizontal axis wind turbine (HAWT) operating in the full-load region, i.e. in the wind speed range between rated wind speed V_{rated} and cut-out wind speed $V_{\text{cut-out}}$. The aerodynamic torque T_a acting on the rotor disk is defined as

$$T_a = \frac{1}{2\omega_r}\rho\pi R^2 C_p(\lambda,\beta)V^3 \tag{1}$$

where ω_r is the rotor speed, ρ the air density, R the blade length, C_p the power coefficient, $\lambda = \frac{\omega_r R}{V}$ the tip-speed ratio, β the pitch angle and V the wind speed. The aerodynamic torque drives the drive-train, which converts the aerodynamic power into electrical power. The drive-train dynamics is defined as follows

$$\dot{\theta}_s = \omega_r - \frac{\omega_g}{N_g} \tag{2a}$$

$$J_r\dot{\omega}_r = T_a - B_d\left(\omega_r - \frac{\omega_g}{N_g}\right) - K_d\theta_s \tag{2b}$$

$$N_g J_g\dot{\omega}_g = B_d\left(\omega_r - \frac{\omega_g}{N_g}\right) + K_d\theta_s - N_g T_g \tag{2c}$$

where θ_s is the torsional angle, ω_g the generator speed, N_g gear ratio, J_g and J_r generator and rotor inertias, K_d and B_d spring and damping coefficients, and T_g the generator torque.

The i-th out-of-plane root bending moment occurs whenever a force acts upon the blade causing it to deflect out of the rotor plane, and it is described by

$$M_{y,i} = \int_0^R r f(r)\,\mathrm{d}r \tag{3}$$

where $f(r)$ is the flap force at the radial distance r from the blade root.

2.2 Individual pitch control

The IPC implementation is pursued according to Bossanyi [2003], using the MBC transformation and two PI controllers. The measured out-of-plane root bending moments or blade loads ($M_{y,i}$) are transformed from the rotating frame into two virtual signals (M_{tilt}, M_{yaw}) in the fixed frame using the MBC

$$\begin{bmatrix} M_{tilt} \\ M_{yaw} \end{bmatrix} = \frac{2}{3}\begin{bmatrix} \cos(n\psi_1) & \cos(n\psi_2) & \cos(n\psi_3) \\ \sin(n\psi_1) & \sin(n\psi_2) & \sin(n\psi_3) \end{bmatrix}\begin{bmatrix} M_{y,1} \\ M_{y,2} \\ M_{y,3} \end{bmatrix} \tag{4}$$

where $\psi_i = \psi + (i-1)\frac{2\pi}{3}$, with ψ being the azimuth angle, and n representing the harmonic (1P, 2P etc.). Then using two identically tuned PI controllers, the pitch angle correction factors are calculated based on the fixed frame moments M_{tilt} and M_{yaw}

$$\beta_j(t) = K_P M_j(t) + K_I\int_0^t M_j(\tau)\,d\tau,\ j\in\{\text{tilt},\text{yaw}\}. \tag{5}$$

Once the fixed frame pitch corrections are computed, they are converted to the rotating frame, using the inverse MBC transformation as shown in (6)

$$\begin{bmatrix} \bar{\beta}_1 \\ \bar{\beta}_2 \\ \bar{\beta}_3 \end{bmatrix} = \begin{bmatrix} \cos(n\psi_1) & \sin(n\psi_1) \\ \cos(n\psi_2) & \sin(n\psi_2) \\ \cos(n\psi_3) & \sin(n\psi_3) \end{bmatrix}\begin{bmatrix} \beta_{tilt} \\ \beta_{yaw} \end{bmatrix}. \tag{6}$$

The commanded pitch angle to each blade actuator is then the sum of the IPC corrections $\bar{\beta}_i$ with the collective pitch signal from the Collective Pitch Control (CPC), i.e. $\beta_i = \beta_c + \bar{\beta}_i$.

2.3 Blade-load sensor topology and faults

It is assumed that individual measurements of out-of-plane root bending moments at each blade are available through a single sensor mounted internally at the blade root, i.e.

$$z_i = M_{y,i} \quad i = 1,2,3. \tag{7}$$

Blade load sensors are sensitive to damage or set-up errors during installation, which may result in incorrect load information from the beginning of a turbine's lifetime. Faults may also develop during operation, where the sensors may begin to detach from the blade root, providing incorrect measurements. The detachment may occur due to changes in the adhesion properties or by the various operational and environmental conditions over time. The sensor readings may also degrade during operation due to another component failing. The previously-mentioned fault types can be modelled as additive and multiplicative. However, due to their frequency of occurrence and the non-linearity they introduce into the system, multiplicative faults are of greater interest. Therefore, the following fault model is assumed for the measurements z_i

$$z_i = \theta_i M_{y,i} \quad i = 1,2,3 \tag{8}$$

where $\theta_i > 0$. This parameter is not upper bounded because the measurements affected by the considered faults may be larger than the actual moment acting on the blade.

3. CONDITION MONITORING

The proposed condition monitoring system consists of a blade load estimator and a statistical change detector. The former provides estimates of the out-of-plane root bending moment for each blade, utilizing estimates of T_a and λ. The latter is comprised of a residual generator that utilizes the estimates $\hat{M}_{y,i}$ and the pitch angles β_i and a detector based on the generalized likelihood ratio test (GLRT). All measured quantities used by the residual generators, namely the i-th pitch angles β_i, generator and rotor angular velocities ω_g and ω_r and the i-th blade load $M_{y,i}$, are affected by Gaussian white noise with mean and variances as specified in Odgaard et al. [2013].

3.1 Residual generation

The moment generated at the blade root highly depends on the local wind speed for the i-th blade, and also the i-th pitch angle computed in response to the wind. Since knowledge of local wind speed is unavailable, an alternative approach is to estimate the Rotor Effective Wind Speed (REWS), which

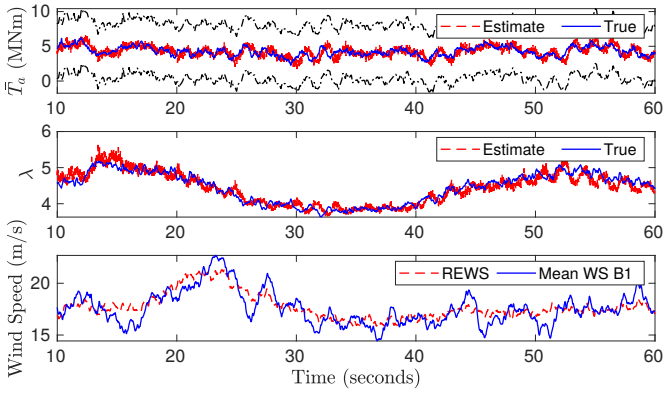

Fig. 1. Estimation of the aerodynamic torque with a 95% confidence interval, estimated TSR and a comparison between the REWS and local mean wind speed.

represents the averaged quantity of the total wind impacting the rotor disk. Soltani et al. [2013] and Jena and Rajendran [2015] reviewed various techniques for REWS estimation, both data-driven and model-based, where the latter typically consists of two steps: aerodynamic torque estimation and then tip-speed/REWS estimation.

Aerodynamic torque estimation. An unknown input Kalman filter based on the drive-train description in (2), augmented with a random walk model, is used to estimate a scaled version of the aerodynamic torque, i.e. $\bar{T}_a = T_a/J_r$ [Song et al., 2017]. The scaling of the aerodynamic torque ensures that all signals are comparable in magnitude, hence the estimator is not affected by large variations in the singular values of the system's dynamical matrix. Figure 1 shows the estimated aerodynamic torque $\hat{T}_a$ in comparison with the true value and the 2.5σ confidence interval based on the a posteriori covariance estimate from the Kalman filter. The estimator tracks variations in T_a, although the rather aggressive tuning of the Kalman filter introduces high frequency variations.

Tip-speed ratio estimation. By using the aerodynamic torque estimate $\hat{T}_a$ it is possible to obtain an estimate of the tip-speed ratio, and by extension, an estimate of the REWS. Equation (1) is an expression for the aerodynamic torque, while assuming collective pitch and uniform wind. However, it must be extended to include information about the individual pitch angles

$$T_a = \frac{\rho\pi R^2}{6\omega_r} V^3 \Big(C_p(\lambda,\beta_1) + C_p(\lambda,\beta_2) + C_p(\lambda,\beta_3) \Big) . \quad (9)$$

An expression containing known quantities on the left-hand side is obtained by isolating the wind speed in tip-speed ratio equation and inserting into (9),

$$\frac{6\hat{T}_a}{\rho\pi R^5 \hat{\omega}_r^2} = \lambda^{-3} \Big(C_p(\lambda,\beta_1) + C_p(\lambda,\beta_2) + C_p(\lambda,\beta_3) \Big) \quad (10)$$

The expression is further reduced by evaluating the power coefficient C_p at the i-th pitch angle,

$$\frac{6\hat{T}_a}{\rho\pi R^5 \omega_r^2} = \hat{\lambda}^{-3} \Big(C_{p,\beta_1}(\hat{\lambda}) + C_{p,\beta_2}(\hat{\lambda}) + C_{p,\beta_3}(\hat{\lambda}) \Big) . \quad (11)$$

It is then possible to solve for the tip-speed ratio $\hat{\lambda}$ in the above equation. Using this together with the estimated rotor angular velocity and the estimated aerodynamic torque, an expression for the REWS is obtained, given as $\hat{V}_{rews} = \frac{R\omega_r}{\hat{\lambda}}$. Figure 1 shows the tip-speed ratio estimation, which captures the overall dynamical trend of the true quantity.

The estimation of the blade load is then pursued using linear regression. The primary factor contributing to the blade load is the local wind speed. Hence, the regression model should make use of inputs carrying information about the wind speed. Both the estimated tip-speed ratio $\hat{\lambda}$ and estimated REWS contain averaged wind speed information, since both quantities describe phenomena occurring within the rotor area. The pitch angles also contain relevant information regarding the wind speed, since the blades are pitched to maintain constant power production in the full-load region. Figure 1 illustrates the estimated REWS compared to the mean local wind speed over one of the three blades. Since the smaller and more rapid wind changes are not captured by $\hat{V}_{rews}$ it is expected that a significant error is introduced in the estimate of the blade loads using either the estimated REWS or the tip-speed ratio in combination with other signals.

Various linear regression models with different input combinations were fitted to the measured out-of-plane root bending moments $M_{y,i}$. The following list contains the associated adjusted R-squared values

- R-squared $= 0.47949$, $\quad \beta_i \rightarrow M_{y,i}$
- R-squared $= 0.48653$, $\quad \beta_i, \hat{\lambda} \rightarrow M_{y,i}$
- R-squared $= 0.49056$, $\quad \beta_i, \hat{\lambda}, \hat{V}_{REWS}, \psi \rightarrow M_{y,i}$
- R-squared $= 0.49552$, $\quad \beta_i, \hat{\lambda}, \beta_i \cdot \hat{\lambda} \rightarrow M_{y,i}$

where the notation $\beta_i \rightarrow M_{y,i}$ denotes the mapping from some input, such as β_i, to the output data $M_{y,i}$. Based on the R-squared values, the main contributing factor is the commanded pitch angle, which was expected, since it is computed in response to changes in wind and load conditions. Inclusion of additional inputs, such as the estimated tip-speed ratio or REWS, has no significant contribution towards the R-squared value. Among the previously considered regression models, the following structure is selected as that one having the largest R-squared

$$\hat{M}_{y,i} = \hat{b}_0 + \hat{b}_1\beta_i + \hat{b}_2\hat{\lambda} + \hat{b}_3\beta_i\hat{\lambda} \quad (12)$$

where $\hat{b}_i$ are the regression coefficients. Figure 2 shows a scatter plot of how the data is distributed compared to the resulting surface described by (12). Figure 3 shows the estimated blade load in comparison with the equivalent measurement: the estimate behaves as expected tracking the overall trend of the blade load, but with a large error due to lack of knowledge regarding local

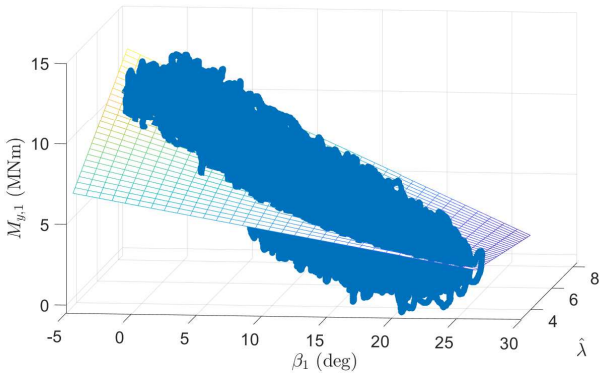

Fig. 2. Scatter plot of the data used for multiple linear regression, compared to the obtained model (the plane).

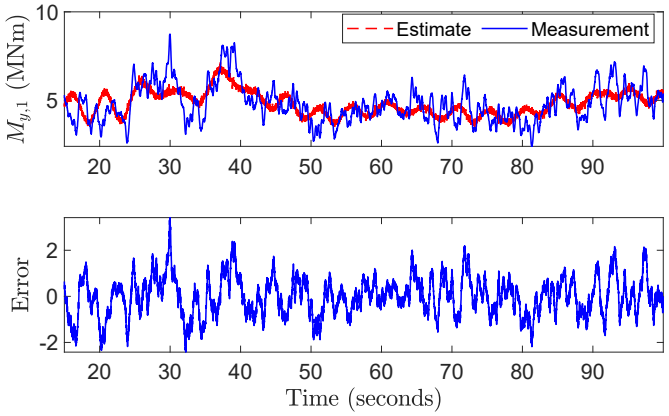

Fig. 3. Estimated blade load using the regression model compared to the measured blade loads (at 18m/s).

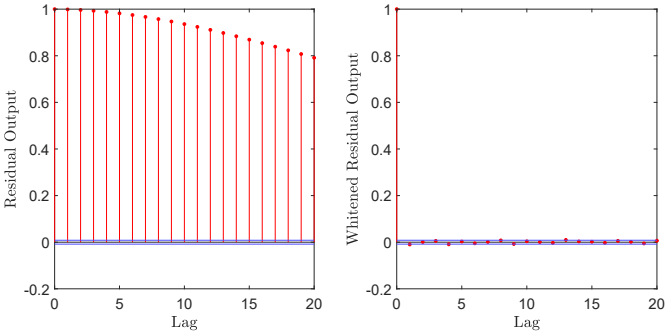

Fig. 4. Comparison of the sampled autocorrelation function of the residual output pre- and post-whitening.

wind speed, which contains information of the rapid and local changes.

Based on the results from the linear regression, the i-th residual for the i-th blade load sensor is generated as follows

$$r_i = M_{y,i,m} - \hat{M}_{y,i} = M_{y,i,m} - \left(\hat{b}_0 + \hat{b}_1\beta_i + \hat{b}_2\hat{\lambda} + \hat{b}_3\beta_i\hat{\lambda}\right) . \quad (13)$$

Since the proposed method relies on the pitch angle and the estimated tip-speed ratio, a fundamental limitation is that the residual is only valid within the full-load region since for $V < V_{\text{rated}}$ pitch control typically ceases.

3.2 Statistical change detection

The design of a condition monitoring system for the blade load sensors is now pursued based on statistical change detection methods and, specifically, the GLRT framework. A fundamental assumption for the development of GLRT-based algorithms is that the residual should be Independent and Identically Distributed (IID) stochastic sequence. The correlation analysis performed on the residuals generated from (13) shows a significant deviation from the whiteness condition. A whitening filter consisting of an ARMA process is therefore designed and applied to the residuals. The correlation structure of r_i before and after whitening is shown in Fig. 4. Once whitened, an appropriate distribution for the residual must be determined. Figure 5 shows a fit of the normal, logistic and t-LocationScale cumulative distribution functions (CDFs) to the whitened residual. Visually, the t-LocationScale distribution is a better approximation for the residual than the Gaussian, since its heavy tails capture the data in low and high ends of the value range. P-values

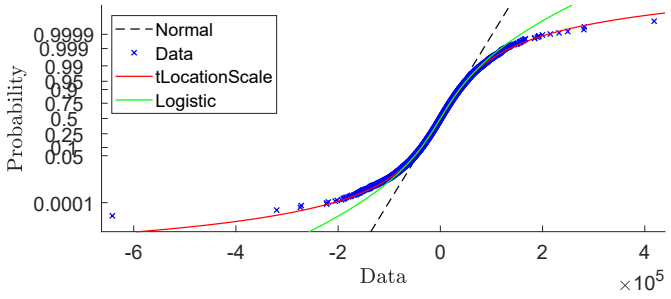

Fig. 5. Fitting distributions to the whitened residual output.

for the whitened residuals were calculated for the Gaussian ($p = 0$), logistic ($p = 0.1417$) and t-LocationScale distributions ($p = 0.7851$), using the Kolmogorov-Smirnov test at 5% significance. The test clearly rejects the hypothesis that the given data is Gaussian; on the other hand the t-LocationScale distribution has the largest p-value, confirming that this distribution is a better fit overall. The probability density function of the t-LocationScale distribution is given by

$$f(x;\mu_t,\sigma_t,\nu_t) = \frac{\Gamma\left(\frac{\nu_t+1}{2}\right)}{\sigma_t\sqrt{\nu_t\pi}\Gamma\left(\frac{\nu_t}{2}\right)}\left[\frac{\nu_t + \left(\frac{x-\mu_t}{\sigma_t}\right)^2}{\nu_t}\right]^{-\left(\frac{\nu_t+1}{2}\right)} \quad (14)$$

with $\Gamma(\cdot)$ being the gamma function, μ_t the location parameter, $\sigma_t > 0$ the scale parameter and $\nu_t > 0$ the shape parameter. The mean of the distribution is equal to the location parameter, whereas the variance is described as

$$\text{var} = \sigma_t^2\frac{\nu_t}{\nu_t - 2} \quad (15)$$

A parameter study was carried out for non-faulty and faulty data to assess which parameters of the distribution are most informative about the considered faulty conditions. As shown in Fig. 6, the multiplicative fault has a clear impact on the mean value of the t-LocationScale distribution, whereas the standard deviation does not provide a distinct change between non-faulty and faulty cases. The shape parameter ν_t remains approximately constant for all cases. Due to the wide range of wind speeds and the stochastic nature of the wind fields, the plots represent the average value of the parameters for a given experiment. Based on this analysis, the monitoring of the blade load sensors is pursued by designing three independent fault detection systems (one for each residual) based on the GLRT algorithm for the t-LocationScale distribution assuming changes of only the location parameter.

Windowed t-LocationScale GLRT. The samples in each of the residual outputs $r_i(k)$ are assumed to be described by the t-LocationScale distribution $r : r_1,\ldots,r_k \sim \mathscr{T}_{iid}(\mu_t,\sigma_t,\nu_t)$. The detection problem is to decide within a given time window M between the null hypothesis $\mathscr{H}_0$ and alternate hypothesis $\mathscr{H}_1$, which are defined as follows,

$$\begin{aligned}\mathscr{H}_0 &: \mu = \mu_0, \quad \text{for} \quad r_i(k), k-M+1 \le i \le k \\ \mathscr{H}_1 &: \mu \neq \mu_0, \quad \text{for} \quad r_i(k), k-M+1 \le i \le k\end{aligned}$$

where μ_0 is the location parameter of the residual distribution in the nominal case. The detector decides the $\mathscr{H}_1$ condition if the following likelihood ratio is larger than the threshold γ

$$L_G(\mathbf{r}) = \frac{\mathscr{T}(\mathbf{r};\hat{\mu},\mathscr{H}_1)}{\mathscr{T}(\mathbf{r};\mu_0,\mathscr{H}_0)} > \gamma \quad (16)$$

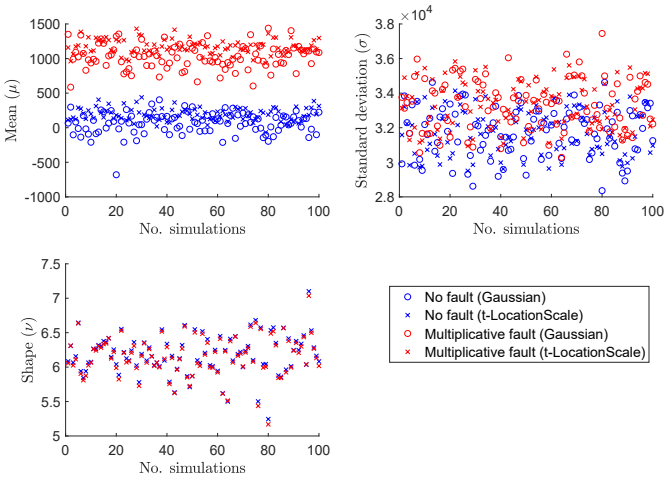

Fig. 6. Comparison between how the parameters of the Gaussian and t-LocationScale distributions change during various fault conditions.

where $\hat{\mu}$ is the maximum likelihood estimate of the location parameter under the hypothesis $\mathscr{H}_1$, and γ is the test threshold for a desired probability of false alarms. Taking the natural log of both sides of (16) the following decision function is obtained

$$g(k) = \left(-\frac{\nu_0+1}{2}\right)\sum_{i=j}^{k}\left\{\ln\left[1+\frac{1}{\nu_0}\left(\frac{r_i-\hat{\mu}}{\sigma_0}\right)^2\right] - \ln\left[1+\frac{1}{\nu_0}\left(\frac{r_i-\mu_0}{\sigma_0}\right)^2\right]\right\} > \gamma' \tag{17}$$

where $\gamma' = \ln\gamma$ and (σ_0, ν_0) are the scale and shape parameters of the t-LocationScale distribution which are invariant across the two hypotheses.

4. SIMULATION

4.1 Simulation framework

All simulations are performed using FASTv8 (NREL [2019]) and are driven by non-uniform stochastic wind fields generated by TurbSim (Jonkman [2009]). The considered wind speed range is only within the full-load region, with speeds of approximately 16-22m/s. The considered wind turbine is the NREL 5MW reference wind turbine defined by Jonkman et al. [2009], where an external controller is required in order to simulate the reference turbine with IPC using FAST. Mulders and van Wingerden [2018] developed the Delft Research Controller (DRC), which provides IPC functionality to FAST. An expansion to the DRC was then developed, in order to provide the ability to inject faults into the control loop.

4.2 Choice of threshold

The decision function output during nominal operation is investigated, in order to choose a suitable threshold (γ'). Figure 7 compares four ensembles of mean wind conditions to their respective Generalized Extreme Value (GEV) distribution fits, with 16m/s being the worst case and, therefore, the considered fit for the threshold computation. It is desired that a significant amount of time passes between false alarms, which in this case is selected as >12 months, which results in a probability of false alarm $P_{FA} = 10^{-8}$ and a threshold of $\gamma' = 5.4858$. Due to

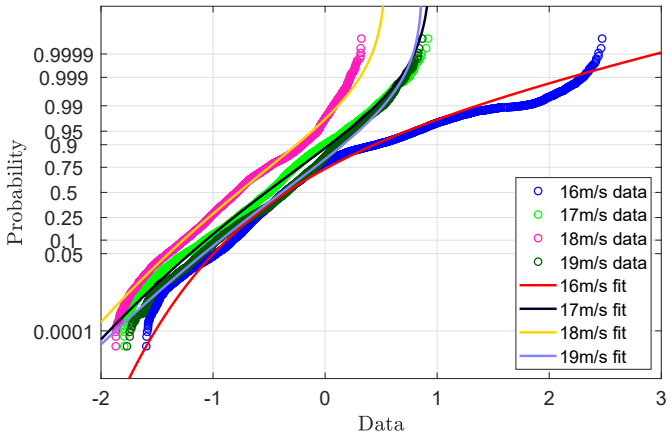

Fig. 7. Probability plot of the decision function under $\mathscr{H}_0$ for four mean wind speeds conditions, with estimated parameters for the Generalized Extreme Value (GEV) distribution.

the small change in location encoutered during the parameter study, a sufficiently large windows size of $M = 62000$ samples is selected in order to ensure detection of a given fault.

4.3 Simulation results

Figure 8 details the occurrence of a multiplicative fault of 0.95, which shows the decision function clearly detecting the fault. Given a situation with multiple multiplicative faults of different magnitudes occurring simultaneously (Fig. 9), the detection scheme clearly captures the two faults. However, part of the performance envelope from the second non-faulty residual also reaches the threshold. This happens due to the residuals being designed as three independent quantities, with their probability of detection and false alarms being considered on a single fault basis. It is also expected due to the fundamental construction of the IPC and residual generators. Since any fault, to some extent, will propagate into each all residuals, because all three measured loads contribute to the virtual M_{tilt} and M_{yaw} moments, which are used to compute the pitch angles. To prevent this issue, the blade load estimation scheme must be independent from the pitch angles. Table 1 showcases the performance of the chosen detection scheme, subject to a fault

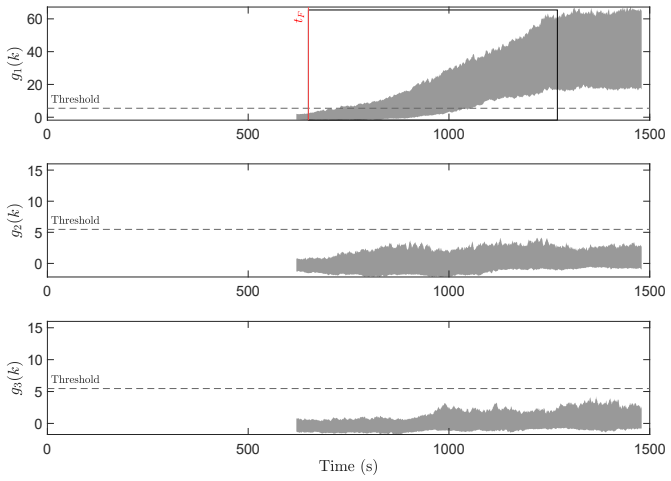

Fig. 8. Performance envelope of $g_i(k)$ during 40 randomly generated wind scenarios within the full load region, with a multiplicative of 0.95 fault occurring at $t = 650s$.

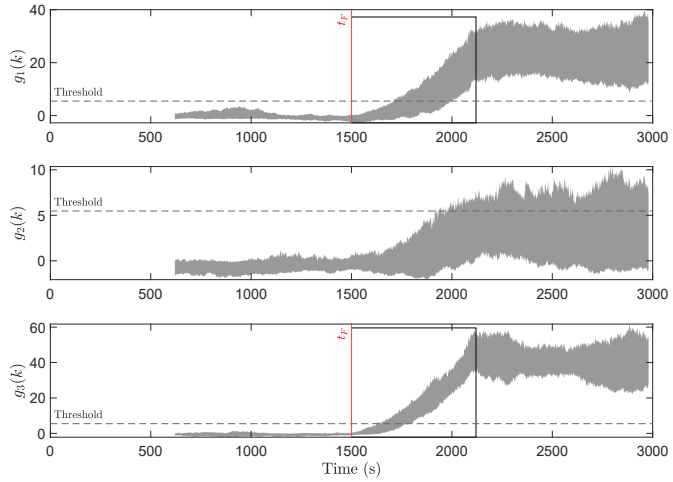

Fig. 9. Performance envelope of $g_i(k)$ during 15 randomly generated wind scenarios with multiplicative faults occurring at $t = 1500s$ of 0.95 on blade 1 and 1.05 on blade 3.

Table 1. Time to detect (t_d) performance in seconds

	Min	Max	Mean	Std
$g(k)$ (0.95)	54	383	220	67
$g(k)$ (1.05)	153	325	251	42

of magnitude 0.95 or 1.05. With a windows size equal to 650s, all the faults in the considered scenarios are comfortably detected.

5. CONCLUSIONS

A scheme for condition monitoring of blade load sensors for single-rotor wind turbines in the full-load region was presented in this paper. The advantage of the proposed method compared to previous approaches pertains to removing the assumption of available local wind speed measurements or scenarios with uniform winds. Blade load estimation was achieved via linear regression based on the tip-speed ratio and pitch angles. Additionally, generalised likelihood ratio tests for a tLocationScale distirbution were utilized to increase robustness of the diagnosis algorithm w.r.t. noise. The efficacy of the proposed method was verified through high-fidelity simulations in realistic scenarios. The obtained results demonstrated that appropriate selection of the window size and threshold for the GLRT can facilitate high probability of fault detection with a low rate of false alarms. The latter requirement was satisfied via systematic selection of the detector threshold based on the statistical properties of the residuals' outputs. A possible extension of the diagnosis scheme that will be able to differentiate between additive from multiplicative faults will be pursued in future studies.

REFERENCES

Bossanyi, E.A. (2003). Individual blade pitch control for load reduction. *Wind Energy*, 6(2), 119–128. doi:10.1002/we.76.

Galeazzi, R., Blanke, M., Falkenberg, T., Poulsen, N.K., Violaris, N., Storhaug, G., and Huss, M. (2015). Parametric roll resonance monitoring using signal-based detection. *Ocean Engineering*, 109, 355–371.

Galeazzi, R., Blanke, M., and Poulsen, N.K. (2012). Early detection of parametric roll resonance on container ships. *IEEE Transactions on Control Systems Technology*, 21(2), 489–503.

Ghane, M., Rasekhi Nejad, A., Blanke, M., Gao, Z., and Moan, T. (2018). Condition monitoring of spar-type floating wind turbine drivetrain using statistical fault diagnosis. *Wind Energy*, 21(7), 575–589.

Hansen, S. and Blanke, M. (2014). Diagnosis of airspeed measurement faults for unmanned aerial vehicles. *IEEE Transactions on Aerospace and Electronic Systems*, 50(1), 224–239.

Jena, D. and Rajendran, S. (2015). A review of estimation of effective wind speed based control of wind turbines. *Renewable and Sustainable Energy Reviews*, 43, 1046–1062.

Jonkman, B.J. (2009). Turbsim user's guide: Version 1.50. Technical report, National Renewable Energy Lab.(NREL), Golden, CO (United States).

Jonkman, J., Butterfield, S., Musial, W., and Scott, G. (2009). Definition of a 5-MW reference wind turbine for offshore system development. Technical Report NREL/TP-500-38060.

Mulders, S. and van Wingerden, J. (2018). Delft research controller: an open-source and community-driven wind turbine baseline controller. *Journal of Physics: Conference Series*, 1037, 032009. doi:10.1088/1742-6596/1037/3/032009.

Niemann, H., Kjølstad Poulsen, N., Mirzaei, M., and Henriksen, L.C. (2018). Fault diagnosis and condition monitoring of wind turbines. *International Journal of Adaptive Control and Signal Processing*, 32(4), 586–613. doi:10.1002/acs.2782.

NREL (2019). FAST - An aeroelastic computer-aided engineering (CAE) tool for horizontal axis wind turbines. URL `https://nwtc.nrel.gov/FAST`. (accessed: 01/11/2019).

Odgaard, P.F., Stoustrup, J., and Kinnaert, M. (2013). Fault-tolerant control of wind turbines: A benchmark model. *IEEE Transactions on Control Systems Technology*, 21(4), 1168–1182. doi:10.1109/TCST.2013.2259235.

Odgaard, P.F., Stoustrup, J., and Kinnaert, M. (2009). Fault tolerant control of wind turbines – a benchmark model. *IFAC Proceedings Volumes*, 42(8), 155 – 160. 7th IFAC Symposium on Fault Detection, Supervision and Safety of Technical Processes.

Sanchez, H., Escobet, T., Puig, V., and Odgaard, P.F. (2015). Fault diagnosis of an advanced wind turbine benchmark using interval-based arrs and observers. *IEEE Transactions on Industrial Electronics*, 62(6), 3783–3793.

Soltani, M.N., Knudsen, T., Svenstrup, M., Wisniewski, R., Brath, P., Ortega, R., and Johnson, K. (2013). Estimation of rotor effective wind speed: A comparison. *IEEE Transactions on Control Systems Technology*, 21(4), 1155–1167.

Song, D., Yang, J., Dong, M., and Joo, Y.H. (2017). Kalman filter-based wind speed estimation for wind turbine control. *International Journal of Control, Automation and Systems*, 15(3), 1089–1096.

Wei, X. and Verhaegen, M. (2011). Sensor and actuator fault diagnosis for wind turbine systems by using robust observer and filter. *Wind Energy*, 14(4), 491–516.

Wei, X., Verhaegen, M., and van den Engelen, T. (2008). Sensor fault diagnosis of wind turbines for fault tolerant. *IFAC Proceedings Volumes*, 41(2), 3222 – 3227. 17th IFAC World Congress.

Willersrud, A., Blanke, M., Imsland, L., and Pavlov, A. (2015). Drillstring washout diagnosis using friction estimation and statistical change detection. *IEEE Transactions on Control Systems Technology*, 23(5), 1886–1900.